

# We are IntechOpen, the world's leading publisher of Open Access books Built by scientists, for scientists

4,800

Open access books available

122,000

International authors and editors

135M

Downloads

Our authors are among the

154

Countries delivered to

TOP 1%

most cited scientists

12.2%

Contributors from top 500 universities



WEB OF SCIENCE™

Selection of our books indexed in the Book Citation Index  
in Web of Science™ Core Collection (BKCI)

Interested in publishing with us?  
Contact [book.department@intechopen.com](mailto:book.department@intechopen.com)

Numbers displayed above are based on latest data collected.  
For more information visit [www.intechopen.com](http://www.intechopen.com)



# Physical Models of Atmospheric Boundary Layer Flows: Some Developments and Recent Applications

*Adrián R. Wittwer, Acir M. Loredó-Souza,  
Mario E. De Bortoli and Jorge O. Marighetti*

## Abstract

Experimental studies on wind engineering require the use of different types of physical models of boundary layer flows. Small-scale models obtained in a wind tunnel, for example, attempt to reproduce real atmosphere phenomena like wind loads on structures and pollutant dispersion by the mean flow and turbulent mixing. The quality of the scale model depends on the similarity between the laboratory-generated flow and the atmospheric flow. Different types of neutral atmospheric boundary layer (ABL) including full-depth and part-depth simulations are experimentally evaluated. The Prof. Jacek Gorecki wind tunnel of the UNNE, Argentina, and the Prof. Joaquim Blessmann closed-return wind tunnel of the UFRGS, Brazil, were used to obtain the experimental data. Finally, some recent wind engineering applications of this type of physical wind models are shown.

**Keywords:** wind tunnel, turbulence, aerodynamic loads, atmospheric dispersion, physical simulation

## 1. Introduction

Wind tunnels are designed to realize similarity in model studies, with the confidence that actual operational conditions will be reproduced. The first step is the evaluation of the flow characteristics with the empty wind tunnel, and then, different flow characteristics are achieved or reproduced at the test section to be applied in the experimental tests. To perform aerodynamic studies of structural models, the distribution of the incident flow must be such that the atmospheric boundary layer (ABL) at the actual location of the structure is reproduced. This is obtained by surface roughness elements and vortex generators, so that natural wind simulations are performed.

The atmospheric boundary layer (ABL) is the lowest part of the atmosphere where the effects of the surface roughness, temperature, and others properties are transmitted by turbulent flows. Turbulent exchanges are very weak when there are conditions of weak winds and very stable stratification [1]. On the other hand, the atmospheric boundary layer over nonhomogeneous terrain is not well defined, and

topographical features could cause highly complex flows. The depth of the atmospheric boundary layer is typically 100 m during the nighttime stable conditions, and this could reach 1 km in daytime unstable conditions [2]. The Prandtl logarithmic law (Eq. (1)), proposed from similarity theories, can be used near the surface in the case of a neutral boundary layer.

$$\frac{U(z)}{u^*} = \frac{1}{0.4} \ln \frac{z - z_d}{z_0} \quad (1)$$

where  $U$  is the mean velocity,  $u^*$  is the friction velocity,  $z_0$  is known as the roughness height, and  $z_d$  is defined as the zero-plane displacement for very rough surface.

The potential law (Eq. (2)) is also widely used in wind engineering to characterize the vertical velocity distribution. The values for the exponent  $\alpha$  vary between 0.10 and 0.43 and the boundary layer thickness  $z_g$  between 250 and 500 m, according to the terrain type [2]. This law is verifiable in the case of strong winds and neutral stability conditions that must be considered for structural analysis.

$$\frac{U(z)}{U(z_g)} = \left( \frac{z}{z_g} \right)^\alpha \quad (2)$$

Similarity requirements corresponding to studies of atmospheric flow in the laboratory can be obtained by the dimensional analysis. The equations are expressed in dimensionless form by means of reference parameters that lead to the following set of non-dimensional groups or numbers: Reynolds number, Prandtl number, Rossby number, and Richardson number. These dimensionless parameters must be in the same value with the model and prototype to obtain the exact similarity, and, in addition, there must be geometric similarity and similarity of the boundary conditions, including incident flow, surface temperature, heat flow, and longitudinal pressure gradient [3].

Geometric scales defined between the simulated laboratory boundary layer and the atmospheric boundary layer are generally <1:200, velocities in the model and prototype have values of the same order, and the viscosity is the same for both cases. This results in the impossibility of reproducing the Reynolds number in low-speed wind tunnels; however, the effects of Reynolds number variation can be taken into account according to the type of wind tunnel test. On the other hand, the equality of the Prandtl number is obtained simply by using the same fluid in model and prototype, as in this case. The equality of the Rossby and Richardson numbers may not be considered for simulation of neutral ABL since Coriolis forces and thermal effects are negligible.

In most laboratories it is more common to simulate the neutrally stratified boundary layer. This implies modeling the distribution of mean velocities, turbulence scales, and atmospheric spectrum [4]. The quality of these approximate models is simply evaluated by comparing the results expressed in dimensionless form with design values. Turbulence intensity distribution is commonly compared with values obtained by other authors [5] and by using Harris-Davenport formula for atmospheric boundary layer [2].

Atmospheric velocity fluctuations with frequencies upper than 0.0015 Hz define the micrometeorological spectral region. Interest of wind engineering is concentrated on this spectral turbulence region. von Kármán suggested an expression for the turbulence spectrum in 1948, and today this spectral formula is still used for wind engineering applications. According to Reference [2], the expression for the dimensionless spectrum of the longitudinal component of atmospheric turbulence is given by Eq. (3):

$$\frac{fS_u}{(u_{RMS})^2} = \frac{1.6(fz_{ref}/U)}{[1 + 11.325(fz_{ref}/U)^2]^{5/6}} \quad (3)$$

where  $S_u$  is the spectral density function of the longitudinal component,  $f$  is the frequency in Hertz, and  $u_{RMS}^2$  is the quadratic mean, or the variance, of the longitudinal velocity fluctuations in  $m^2/s^2$ . The dimensionless frequency  $fz_{ref}/U$  is defined using an appropriate  $z_{ref}$ , generally gradient height, and the mean velocity  $U$ .

Different boundary layer flows are experimentally analyzed in this work. First, three types of boundary layer flows developed at the UNNE wind tunnel: one corresponding to a naturally developed boundary layer with the empty wind tunnel and the other two generated by different ABL simulation methods. Then, simulated ABL flows obtained with different velocities at the UFRGS wind tunnel are analyzed, and the results are compared with each other. Finally, some recent applications of ABL simulations are described, among them wind effects in high-rise buildings considering the urban environment and the surrounding topography, low buildings, aerodynamics of cable-stayed bridges, pollutant atmospheric dispersion, and flow in the wake of wind turbines.

## 2. Boundary layer flows at the UNNE wind tunnel

Next, measurement results obtained at the Prof. Jacek Gorecki wind tunnel of the UNNE (**Figure 1**) in three different boundary layer flows are analyzed. The UNNE wind tunnel is a 39.56-m-long channel where the air enters through a contraction to reach the test section. This is connected to the velocity regulator and to the blower, and then, the air passes through a diffuser before leaving the wind tunnel. The contraction has a honeycomb and a screen to uniform the airflow. The test section is a 22.8-m-long rectangular channel (2.40 m width, 1.80 m height) where two rotating tables are located to place test models. Conditions of zero-pressure-gradient boundary layers can be obtained by the vertical displacement of the upper wall. The blower has a 2.25 m diameter and is driven by a 92 kW electric motor at 720 rpm.

The first of these flows correspond to a boundary layer developed on the smooth floor of the wind tunnel test section. Then, the results obtained for two ABL simulations are analyzed. The first model corresponds to a full-depth simulation of the neutrally stable ABL and the second to a part-depth model.



**Figure 1.**  
The Prof. Jacek Gorecki boundary layer wind tunnel of the UNNE.

Velocity and longitudinal velocity fluctuations were measured by a Dantec 56C constant temperature hot-wire anemometer connected to a Stanford amplifier with low- and high-pass analogic filters. Hot-wire signals were digitalized by a DAS-1600 A/D converter board controlled by a computer which was also used for the analysis of the results. Voltage output from hot wires was converted in mean velocity and velocity fluctuations [6, 7] by the probe calibration curves previously determined. Full spectra from longitudinal velocity fluctuations were obtained by juxtaposing three different partial spectra from three different sampling series, registered in the same location, each with a specific sampling frequency, designed as low, mean, and high frequencies. Then, the fast Fourier transform (FFT) algorithm was applied to each numerical series, and the corresponding longitudinal turbulence spectra were obtained.

## 2.1 The boundary layer obtained with empty tunnel

The uniformity of the flow corresponding to the empty boundary layer wind tunnel is evaluated previously to implement physical models of turbulent flows. Deviations of mean velocity and turbulence intensity are measured to determine uniform flow zones and boundary layer thickness in the test section. Finally, longitudinal component of the turbulence spectrum is obtained from the boundary layer flow and from the uniform flow.

Dimensionless velocity profiles measured with the empty tunnel along a vertical line on the center of the rotating table of the test section (see reference [8]) and at positions 0.6 m to the right and left of this line are presented in **Figure 2**. The vertical coordinate  $z$  is measured from the floor, and  $H$  is the test section height equal to 1.80 m. Measurements are presented only for the lower half of the test section. The depth of the boundary layer is of about 0.3 m, and a good uniformity can be observed from the vertical velocity distributions. A maximal deviation of the mean velocity of about 3% is verified outside the boundary layer, by taking the velocity at the center of the channel as reference.

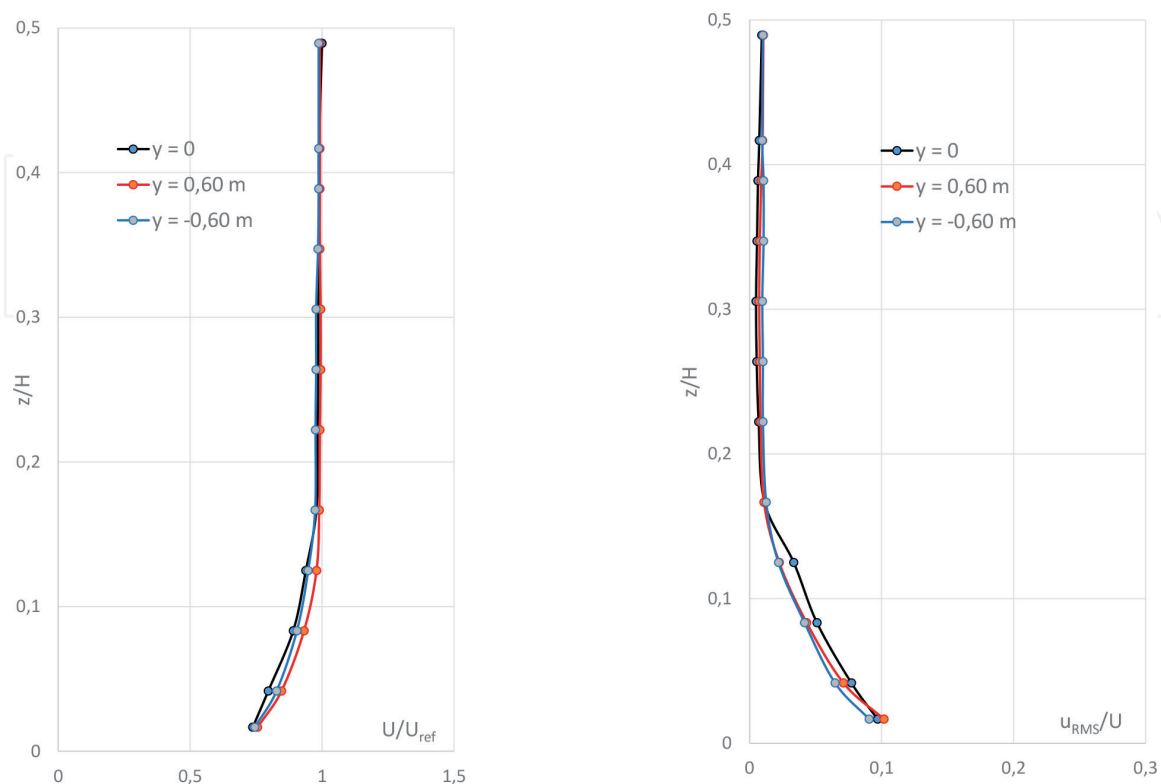


**Figure 2.** Vertical profiles of mean velocity and turbulence intensity with the empty wind tunnel.

Turbulence intensity distribution at the same locations shows values around 1% outside the boundary layer increasing, as expected, inside the boundary layer. Reference velocity for these tests was the velocity at the center of the channel, 27 m/s. The value of Reynolds number calculated with the hydraulic diameter of the test section was  $3.67 \times 10^6$ .

Turbulence spectra obtained inside and outside the boundary layer with the empty tunnel are presented in **Figure 3**. Inside the boundary layer, it is possible to observe higher values of fluctuation energy and a clear definition of the 5/3 declivity, characterizing Kolmogorov's inertial subrange. Outside the boundary layer, low turbulence levels produce a spectral definition only for frequencies minor than 70 Hz.

## 2.2 Full-depth simulation of the atmospheric boundary layer

The complete boundary layer thickness of the ABL is simulated when a full-depth simulation is developed. The Counihan method [9] was applied at the UNNE wind tunnel, and four 1.42-m-high elliptic vortex generators and a 0.23 m (b) barrier were used, together with prismatic roughness elements placed on the test section floor along 17 m (see **Figure 4**).

Velocity and longitudinal velocity fluctuations were measured by the same hot-wire anemometer system described above. Measurements of the mean velocity distribution were made along a vertical line on the center of rotating table and along lines 0.30 m to the right and left of this line. **Figure 5** shows the vertical velocity distribution, and at center, the same measured values are presented in a log-graph to verify the low part of the profile where the distribution of mean speeds is logarithmic. There is a good similarity among the three measured velocity profiles, and the value of the exponent  $\alpha$  obtained by fitting to Eq. (2) is 0.24.

Turbulence intensity distribution at the same locations is also shown in **Figure 5** on the right. The values are lower than those obtained by using Harris-Davenport formula for atmospheric boundary layer [2]. This behavior was verified by other authors [5] mainly in the points located above ( $z/H > 0.5$ ).

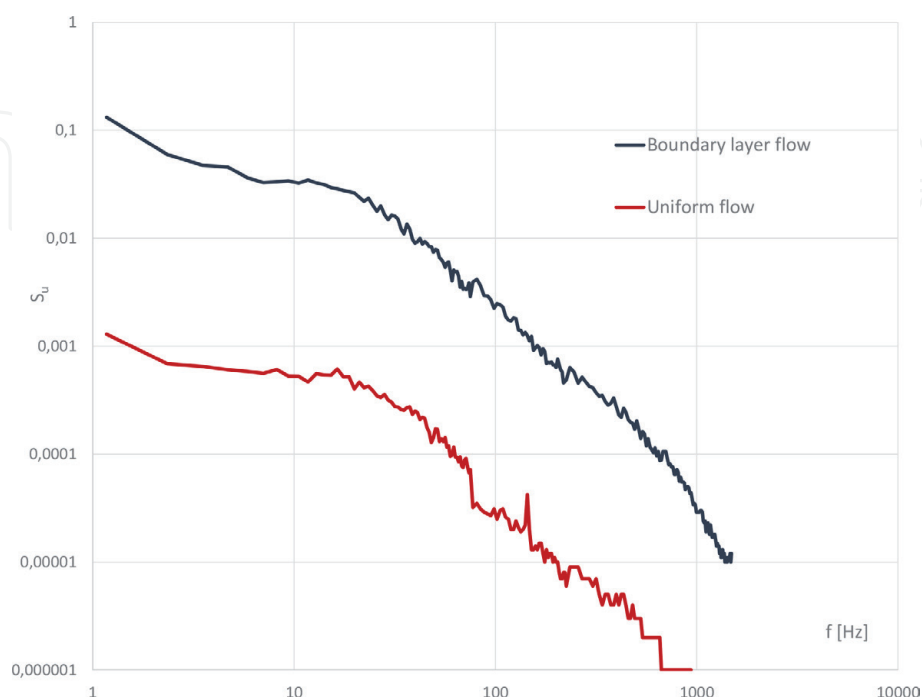


**Figure 3.**  
*Spectral density function with the empty wind tunnel.*



**Figure 4.**  
Counihan vortex generators, barrier, and roughness elements of the full-depth boundary layer simulation.

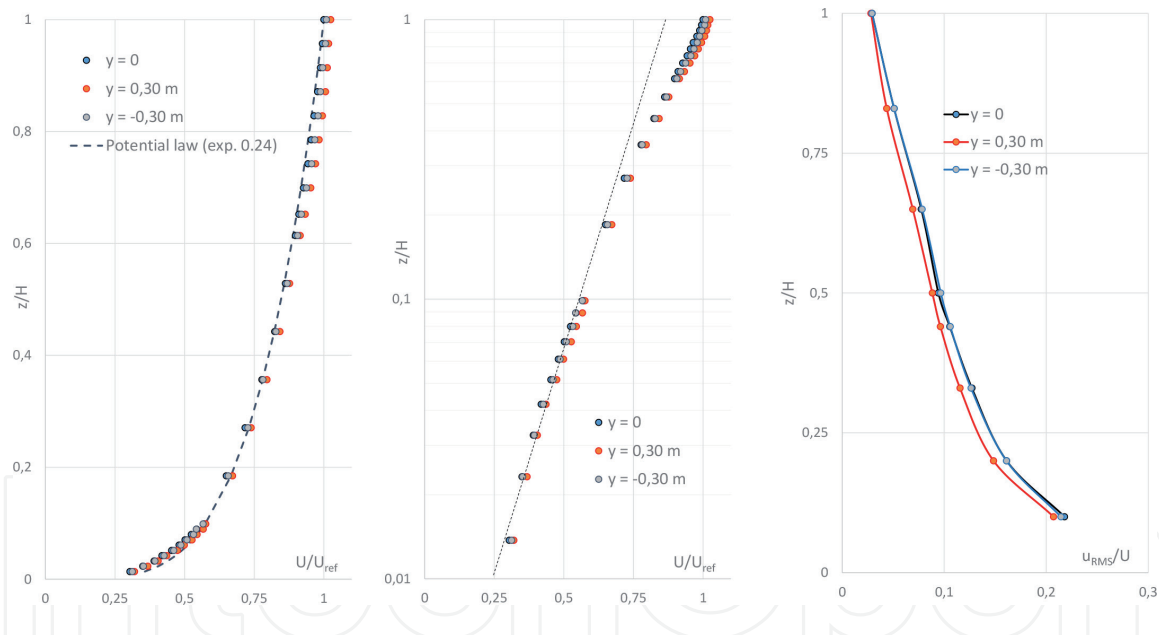


**Figure 5.**  
Vertical mean velocity and turbulence intensity profiles measured for the full-depth boundary layer simulation.

Three spectra obtained at positions  $z = 0.23, 0.58, \text{ and } 0.97 \text{ m}$  are presented in **Figure 6**. An important characteristic of the spectra is the presence of a clear region of the Kolmogorov's inertial subrange. The comparison of the results obtained through the simulations with the atmospheric boundary layer is made by means of dimensionless variables of the auto-spectral density and of the frequency using the von Kármán spectrum (Eq. (3)). A good agreement is observed at  $z = 0.23 \text{ m}$ , but this agreement diminishes at positions  $z = 0.58 \text{ and } 0.97 \text{ m}$ , and this behavior is coincident with the behavior observed for the turbulence intensities.

These measurements were realized at velocity  $U_{ref} \approx 27 \text{ m/s}$ , being  $U_{ref}$  measured at gradient height  $z_g = 1.16$  and the corresponding Reynolds number value of  $Re \approx 2.10 \times 10^6$ . A scale factor of 250 was calculated through the Cook's procedure [5], using the roughness length  $z_0$  and the integral scale  $L_u$  as key parameters. The

value of the roughness length was obtained by fitting mean velocity values to the logarithmic law, and the integral scale values were determined through the fitting of the measured spectrum to the design spectrum.

### 2.3 Part-depth simulation of the atmospheric boundary layer

Two Irwin-type generators separated 1.5 m were used to simulate the part-depth boundary layer by means of the Standen method [10]. The windward plate of the

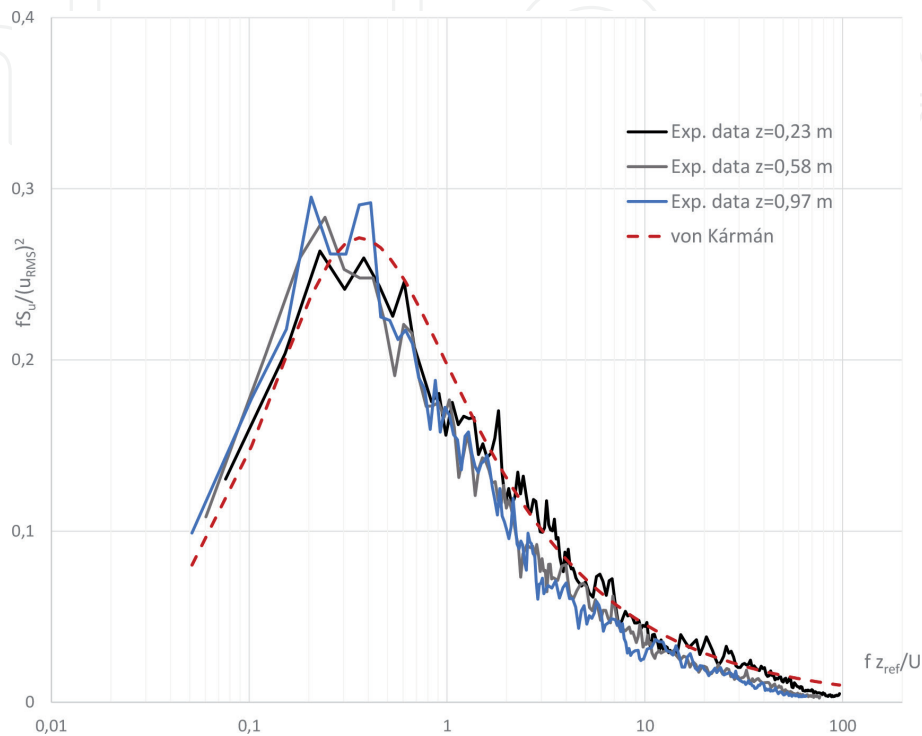


**Figure 6.**  
*Dimensionless spectra obtained at different heights for the full-depth boundary layer simulation and the von Kármán spectrum.*



**Figure 7.**  
*Irwin vortex generators and roughness elements of the part-depth boundary layer simulation.*



simulator has a trapezoidal shape of 1.50 m height, 0.53 and 0.32 m sides. The roughness elements distributed on the test section floor is the same that was used for the Counihan method (**Figure 7**).

Measurements of mean velocity and longitudinal velocity fluctuations were made along a vertical line on the center of rotating table and along lines 0.60 m to the right and left of this line. Vertical velocity distribution and the corresponding log-graph representation to verify the extension of the logarithmic behavior are shown in **Figure 8**. The three measured velocity profiles are quite similar, and the fit to Eq. (2) determines a value of the exponent  $\alpha$  of 0.23.

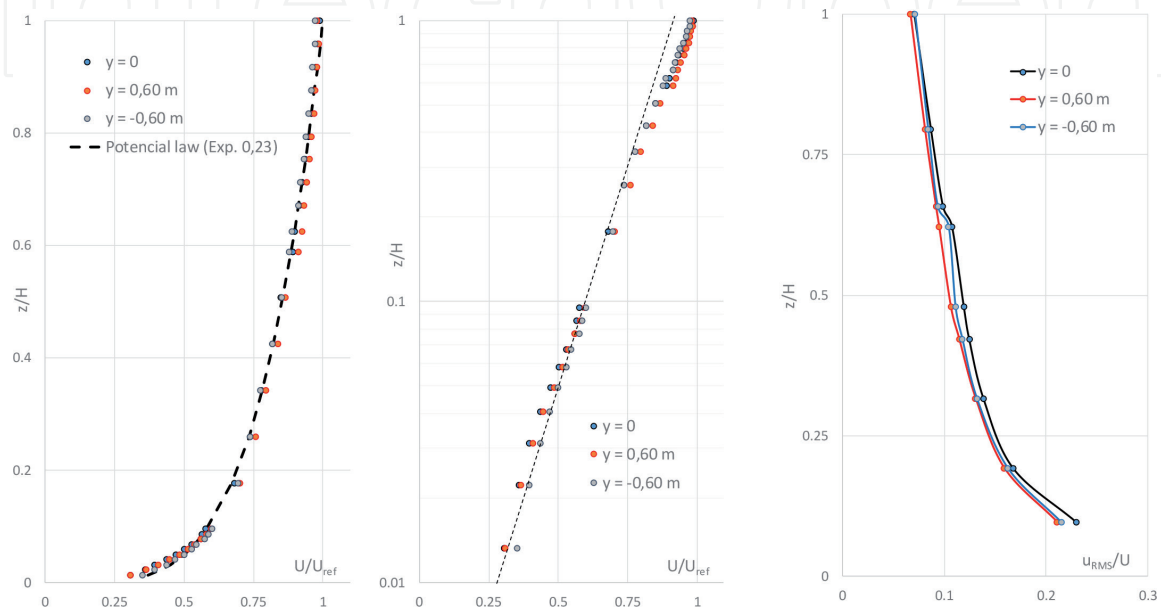


**Figure 8.**

Vertical mean velocity and turbulence intensity profiles measured for the part-depth boundary layer simulation.

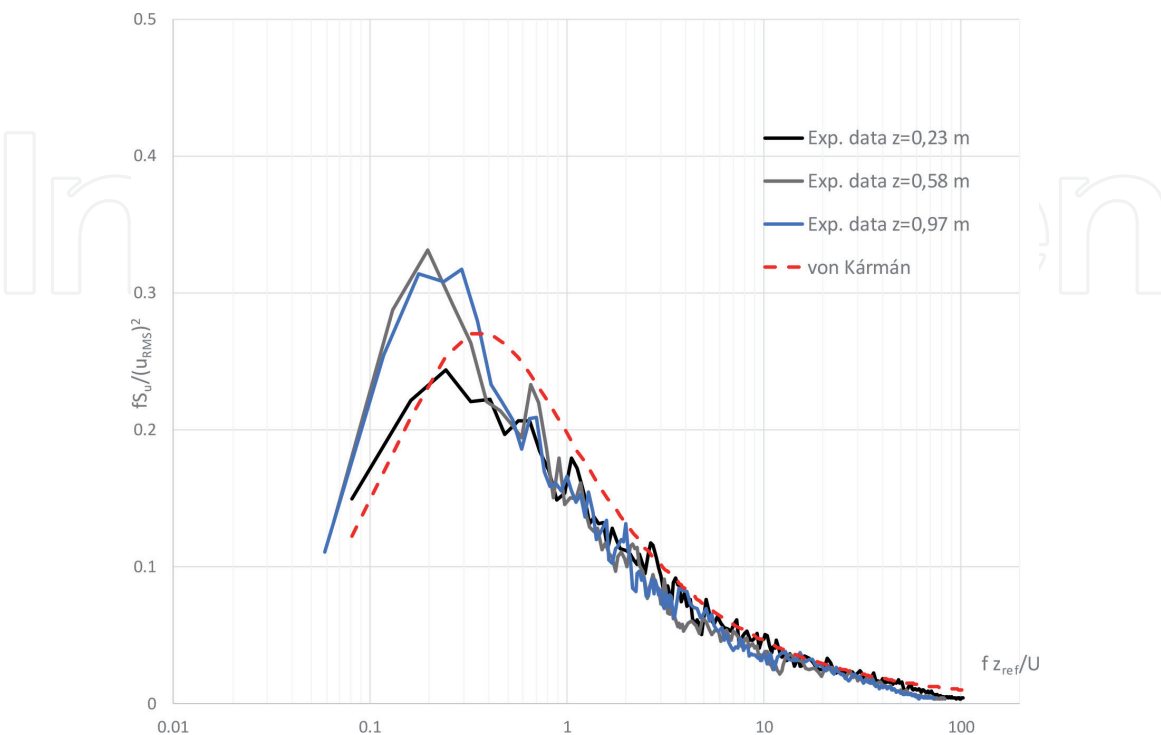


**Figure 9.**

Dimensionless spectra obtained at different heights for the part-depth boundary layer simulation and the von Kármán spectrum.

**Figure 8**, to the right, also shows turbulence intensity distribution at the same locations. The values are higher than those obtained by full-depth boundary layer, mainly in the positions located above, but lower than those obtained using Harris-Davenport formula if the condition of part-depth is considered. However, higher turbulence levels in these positions indicate a coherent behavior when a part-depth ABL is simulated.

**Figure 9** has shown spectra obtained at positions  $z = 0.23, 0.58,$  and  $0.97$  m. Dimensionless spectral comparison indicates a shift of the experimental peak toward low frequencies with respect to the von Kármán spectrum. Higher differences of energy contents are also observed between the spectrum obtained at  $z = 0.23$  m and spectra measured at upper positions.

The reference velocity for these tests was  $U_{ref} \approx 25.5$  m/s and the gradient height  $z_g = 1.21$  m. The corresponding Reynolds number value of  $Re \approx 2.01 \times 10^6$ . Finally, the Cook's procedure [5] was applied, and a scale factor of 150 was calculated.

### 3. Boundary layer flows at the UFRGS wind tunnel

Next, tests made at the wind tunnel of the UFRGS (**Figure 10**) are analyzed. The Prof. Joaquim Blessmann boundary layer wind tunnel at the Laboratório de Aerodinâmica das Construções of UFRGS, Brazil, is a closed-return circuit, and it has a cross-section of  $1.30 \text{ m} \times 0.90 \text{ m}$  at downstream end of the main working section that is  $9.32 \text{ m}$  long (**Figure 10**). A detailed description of the characteristics of the tunnel is indicated in Blessmann's previous work [11].

#### 3.1 Simulation of atmospheric boundary layers with different velocities

Four perforated spires, a barrier, and surface roughness elements were used to simulate a full-depth boundary layer. The arrangement of the simulation hardware is shown/illustrated in **Figure 11**. Velocity and longitudinal velocity fluctuations were measured by means of a TSI hot-wire anemometer along a vertical line on the center of rotating table located downstream of the working section.



**Figure 10.**  
*The Prof. Joaquim Blessmann boundary layer wind tunnel of the UFRGS.*

**Figure 12** shows the non-dimensional profiles obtained with low velocities  $U_{ref} = 1$  and 3.5 m/s, respectively. These profiles are compared with the values obtained with the highest mean velocity achievable in the wind tunnel ( $U_{ref} \approx 35$  m/s). The mean velocity profile given by the power law expression (Eq. (2)) is also included in this graph, being the power law exponent  $\alpha$  equal to 0.23 and the boundary layer thickness  $H = 0.60$  m.

Also, turbulence intensities measured in correspondence to  $U_{ref} = 1, 3.5,$  and 35 m/s are shown in **Figure 12**. Turbulence intensity values corresponding to 3.5 m/s are slightly higher than those obtained at high velocity, which is a behavior commonly observed at low velocities. For measurements at velocity  $U_{ref} = 1$  m/s, it is possible to observe even larger deviations in comparison with 3.5 and 35 m/s cases that can be attributed to extremely low velocity. It is worth noting that with these velocity magnitudes, the relative errors affecting the hot-wire anemometer technique are larger than for measurements at high velocities. This kind of measurement deviation was also observed in similar wind tunnel tests using three-dimensional laser Doppler velocimetry [12].

Power spectra of the velocity fluctuations obtained at two different positions,  $z = 0.15$  and 0.35 m with low velocities  $U_{ref} = 1$  and 3.5 m/s, respectively, are presented in **Figure 13**. Sampling series used for the spectral analysis were obtained with an acquisition frequency of 1024 Hz. A poor definition of the Kolmogorov's inertial subrange is observed for the spectra measured at velocity  $U_{ref} = 1$  m/s.

### 3.2 Analysis of the model scale factor

The evaluation of the model scale factor was only realized with high velocity  $U_{ref} = 35$  m/s. The Cook's procedure [5] was applied using the form proposed by Blessmann [11] and a value of the scale factor at each measurement position by means of the roughness length  $z_0$  and the integral scale  $L_u$ . Finally, a mean value of the model scale factor of 400 was calculated, and it is considered the same in the case of low velocities based on the maintenance of the mean statistical parameters.

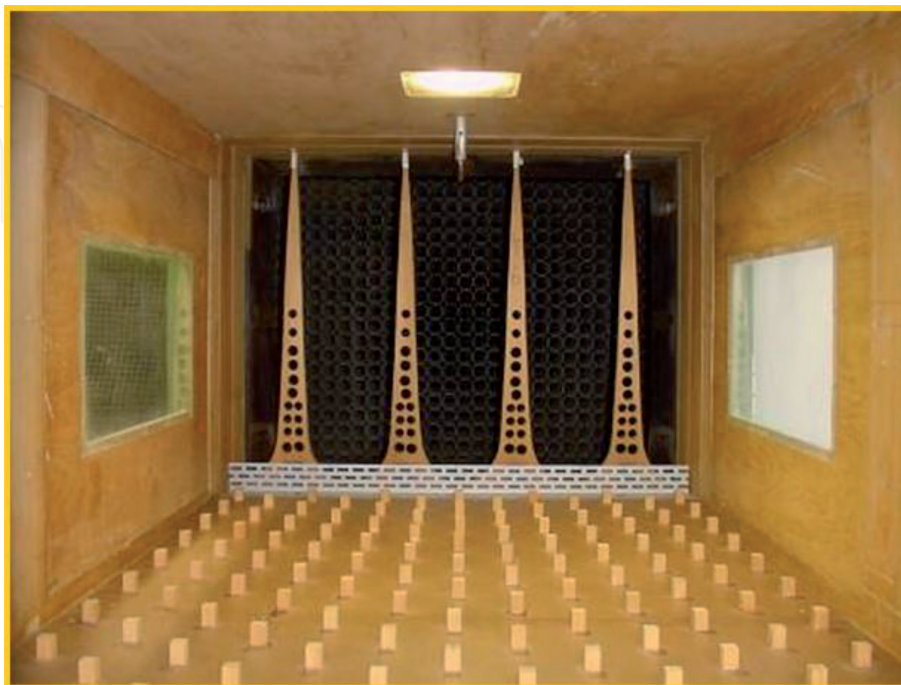


**Figure 11.** Perforated spires, barrier, and roughness elements to simulate a full-depth atmospheric boundary layer.

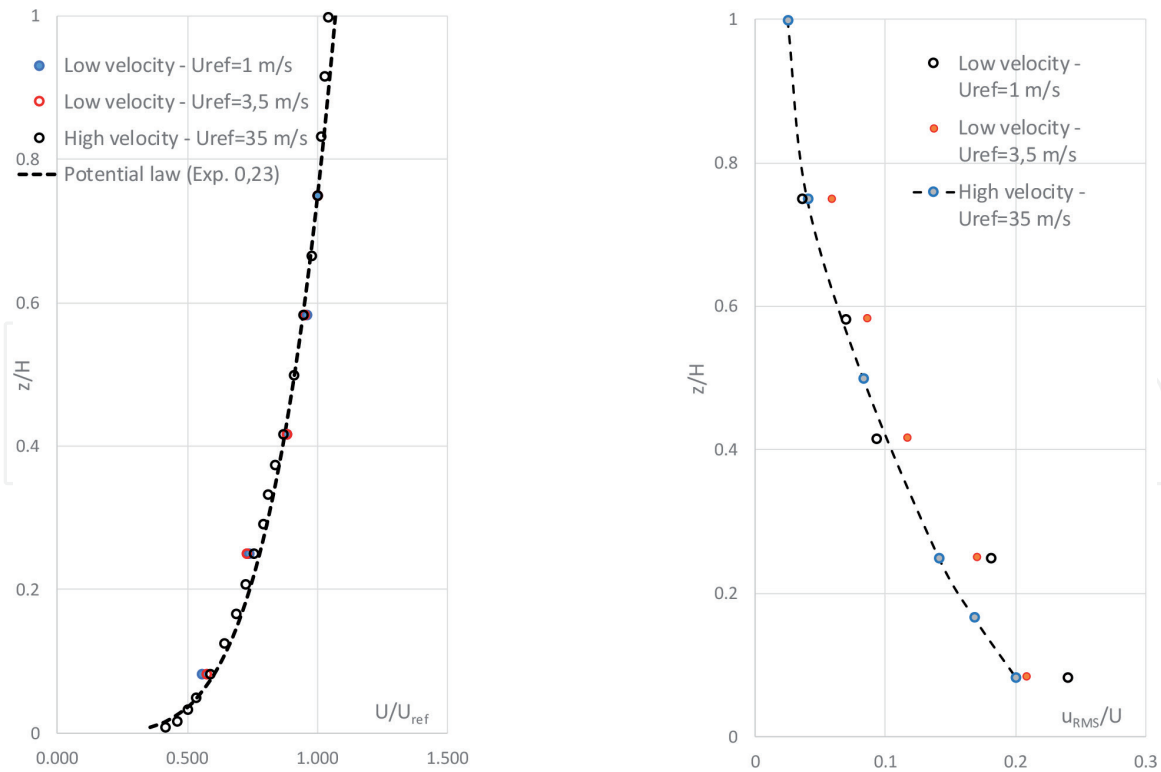


**Figure 12.** Vertical mean velocity and turbulence intensity profiles measured with different reference velocities for a full-depth boundary layer simulation.

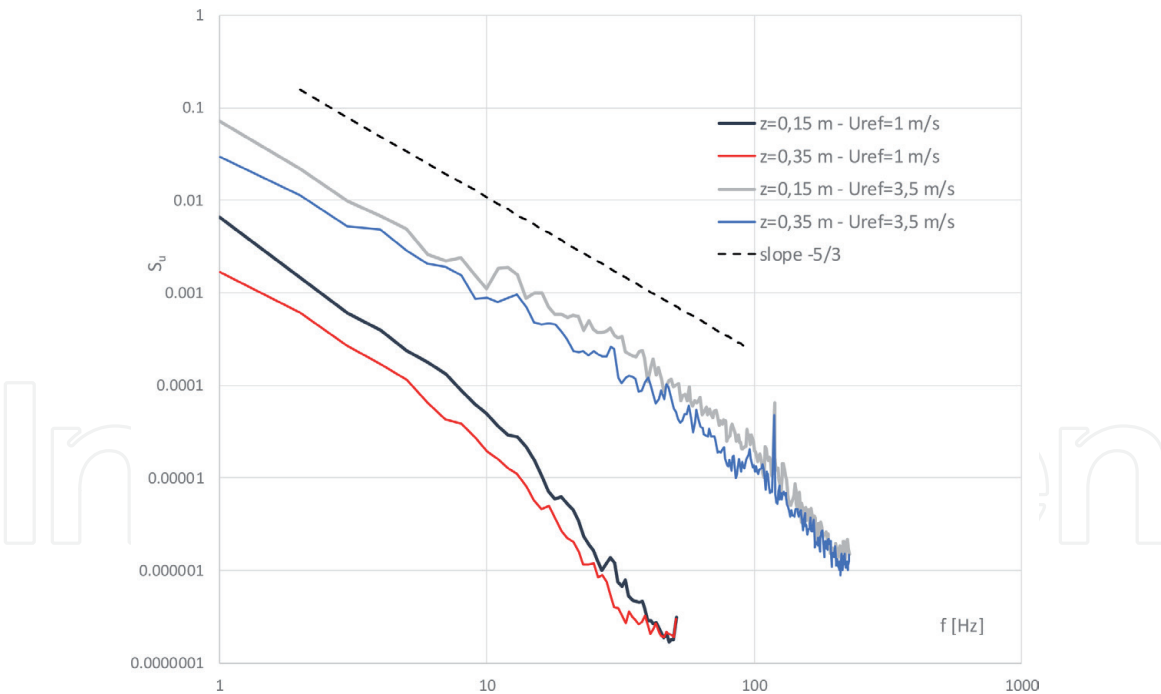


**Figure 13.** Spectral density function measured with low velocity at two positions  $z = 0.15$  m and  $0.35$  m for a full-depth boundary layer simulation.

#### 4. Recent applications of simulated boundary layer flows

Some recent wind engineering applications of the ABL simulations are presented. In general, this type of applications was referred to wind action on civil structures, but new studies related with ambient evaluation, urban design, and wind energy are being developed. In this work, experimental studies related to

high-rise and low building, atmospheric pollutant dispersion, rain-wind action on structures, and the turbulent wake of wind turbines will be shown.

#### 4.1 Wind tunnel study of the local aerodynamic loads on a high-rise building

A study of the wind loads on a high-rise building was realized in the Prof. Jacek Gorecki wind tunnel using a 1/400 scale model [13]. The building is 240 m high; it is named Infinity Tower and it is built in Camboriu, RS, Brazil. Local mean, maximum, minimum, and *rms* pressure coefficients were measured by means of a Scanivalve pressure system.

Atmospheric boundary layer simulations similar to the full-depth simulation described in Section 2.2 were used. Some characteristics of the incident wind were modified according to the terrain features upwind model. Thus, two different mean velocity profiles were used according to the incident wind direction. Aerodynamic details were reproduced in the building model (**Figure 14**), and fluctuating local pressures in 511 tower points for 24 wind directions were measured. The effects of urban vicinity and topographic surrounding were considered by means of a detailed modeling.

Some considerations referred to the extreme values approximation were realized in this work. The graph in **Figure 14** illustrates a fluctuating pressure registered at a measurement point. Mean values associated with different duration times of wind gusts (1, 4, and 16 s full-scale) can be obtained by means of this technique, and statistical extreme value analysis can be applied to improve the calculation of local wind loads.

#### 4.2 Wind tunnel study of the aerodynamic loads on a low structure

There exist structures that due to its size, complexity, or importance justify turning to wind tunnel tests in order to optimize the structural design. A wind tunnel study of the Ezeiza Airport located in that village of Buenos Aires was realized in 2010 [14]. The study comprised the determination of both local and global wind actions.

It was carried out at the Prof. Jacek Gorecki wind tunnel of the UNNE, using different 1/200 scale models (**Figure 15**) that were compatible with the scale factor of the wind simulated in the wind tunnel. The real neighbor conditions were taken into account as well as the turbulent features of the atmospheric wind in agreement with the type of terrain. In this case, an ABL flow similar to the part-depth simulation described in Section 2.3 was used.

In addition to the mean load coefficients, peak coefficients were obtained by extreme value analysis using the Cook and Mayne method [15]. It is shown how

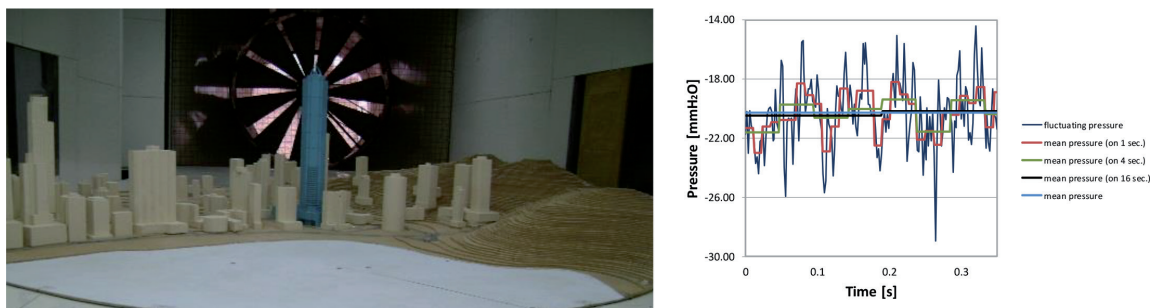


**Figure 14.** High-rise building scale model in the test section of the UNNE wind tunnel and detail of the fluctuating local pressure.

the application of this kind of analysis is influenced in this particular case and, in general terms, how the design of structures could be optimized by means of this kind of studies.

### 4.3 Aerodynamic analysis of cable-stayed bridges

The prediction of the aerodynamic performance of concrete cable-stayed bridges can be realized by means of wind tunnel testing. The analyses of the structural stability under the aerodynamic actions must be included into the design verifications. The structural characteristics of cable-stayed bridges and the dynamic aspects of the aerodynamic actions implicate the application of special analyses of aerodynamic stability including flutter and vortex shedding. The determination of the critical velocity is very important in the design of cable-stayed bridges.

First, static forces are obtained through force balance measurements for simple models of the bridge deck and towers. Aerodynamic coefficients varying with wind incidence for the deck may be easily measured with pressure systems or force balance.

A sectional model is used for the dynamic modeling of the deck. The sectional model must be ideally rigid to avoid the influence of the own model vibration in the experimental results. Details of the bridge deck must be represented. **Figure 16**, left, shows a picture of a 1:60 dynamic sectional model mounted in the test section of the wind tunnel of Prof. Joaquim Blessmann of the UFRGS. The deck corresponds to the Octávio Frias de Oliveira cable-stayed bridge, and the obtained results permitted to observe the differences in the deck vertical and torsional responses [16].

The relevant parameters in aeroelastic modeling are length, specific mass (density), and acceleration. The design of a full-aeroelastic model must reproduce the aerodynamic and dynamic characteristics of the structure of interest. The flow and geometric similarities must be respected and the Reynolds number considered for aerodynamic similarity. The most relevant frequencies and mode shapes must be reproduced to obtain dynamic similarity. The design of full-aeroelastic model includes bridge deck, cables, masts, and end supports. The complexity of this type of model can be observed in **Figure 16**, right, showing the full-aeroelastic model, the Octávio Frias de Oliveira cable-stayed bridge tested at the wind tunnel Prof. Joaquim Blessmann of the UFRGS [17].

The incident wind used to test sectional models is normally a turbulent uniform flow similar to the flow obtained with empty tunnel out the wall boundary layer and described in Section 2.1. Meanwhile, the full-aeroelastic model of the Octávio Frias de Oliveira cable-stayed bridge was tested using a full-depth boundary layer simulated

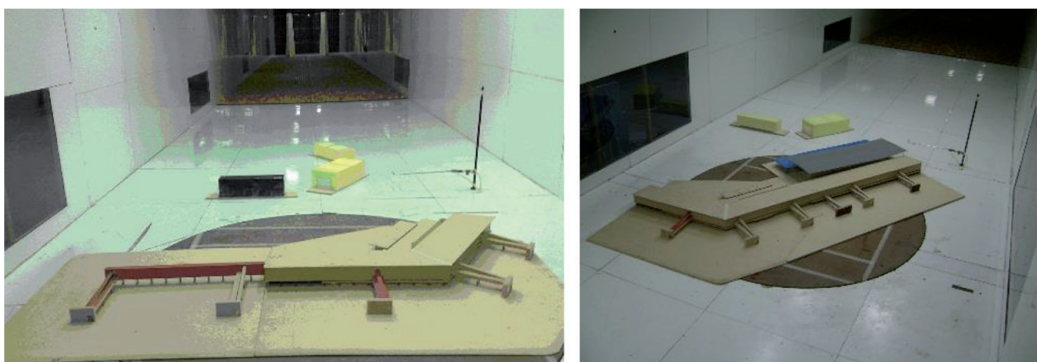


**Figure 15.**  
*Ezeiza Airport 1/200 models (partial) in the test section of the UNNE wind tunnel.*

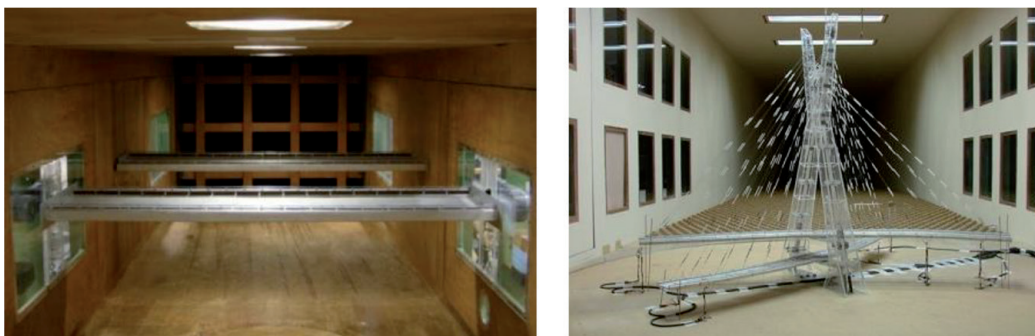


**Figure 16.** Sectional model and full-aeroelastic model of the Octávio Frias de Oliveira cable-stayed bridge in the wind tunnel Prof. Joaquim Blessmann.

in the return section of the wind tunnel Prof. Joaquim Blessmann. The simulation devices and roughness elements are similar to those described in Section 2.2.

#### 4.4 Study of atmospheric dispersion by means of scale model

The concentration fields in the proximities of a local gas emission source were experimentally analyzed in several combinations of wind incidences and source emissions. Concentration measurements were performed by an aspirating probe in a boundary layer wind tunnel. The analysis included the mean concentration values and the intensity of concentration fluctuations in a neutral atmospheric boundary layer flow [18–20].

To perform atmospheric diffusion studies, it is usual to consider full-scale wind speeds in the range of 5–20 m/s [21]. Thus, in order to fulfill the Froude number similarity, the wind tunnel modeling must be performed at low free-stream mean velocities. Atmospheric boundary layer developed with low mean velocities similar to the full-depth simulations described in Section 3.1 was used in the UFRGS wind tunnel.

The hot-wire anemometer, by incorporating the aspirating probe, becomes a density measurement system, and when binary gas mixtures are used, the system measures instantaneous concentrations. A gas mixer was used to provide known air-helium mixtures to calibrate the probe [22]. This type of probe produces a wide useful bandwidth of frequency response, and it allows the evaluation of the plume fluctuating concentration near the source in a turbulent wind. At each measurement point, a sample of 1 min was taken at a sampling frequency of 1024 Hz.

Different configurations were tested in the wind tunnel of Prof. Joaquim Blessmann of the UFRGS, but in this work only the case of an isolated stack in a homogeneous terrain is shown in partial form (**Figure 17**). The results obtained are presented as profiles of concentration coefficient  $K$  and intensity of the concentration fluctuations  $I_c$ , being  $K = CU_H H^2 / Q_0$  and  $I_c = \sigma_c / C$ , where  $C$  and  $\sigma_c$  are the mean concentration and the standard deviation (rms) of the concentration fluctuations, respectively,  $Q_0$  is the total exhaust volume flow rate ( $\text{m}^3/\text{s}$ ),  $U_H$  is the wind velocity at the emission source height (stack height), and  $z$  is the vertical coordinate measured from the wind tunnel floor.

**Figure 18** presents vertical profiles of concentration coefficient  $K$  and  $I_c$  for a specific condition of emission where plume velocity ratio is 0.66, plume momentum is 0.060, and the buoyancy parameter is  $-0.031$ . The experimental mean concentration values are contrasted with Gaussian profiles. It was possible to highlight the observation of the plume vertical asymmetry in the case of an isolated emission source and different probabilistic behavior of the concentration fluctuation data in a cross-sectional measurement plane inside the plume.

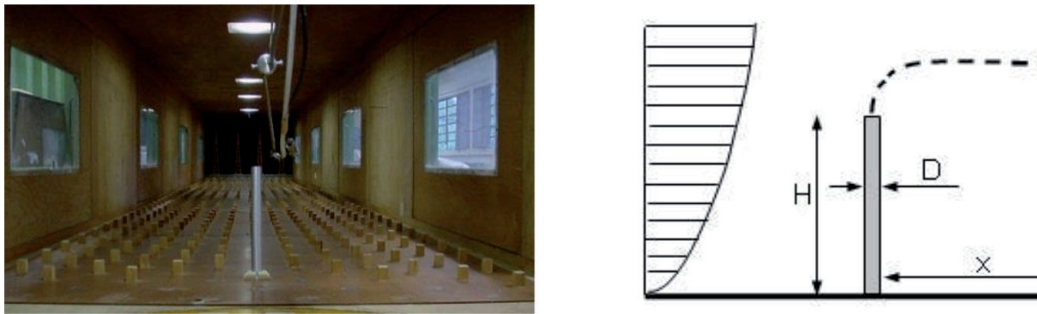


**Figure 17.**  
 Isolated emission source model in the test section of the UFRGS wind tunnel.

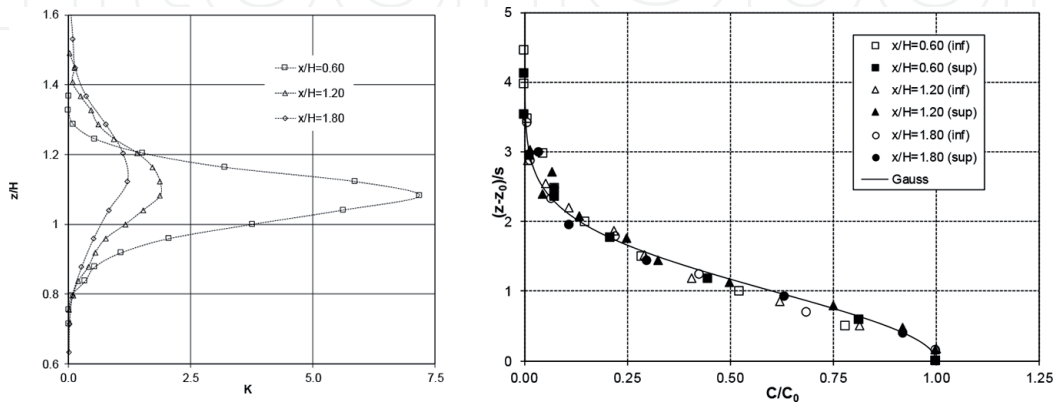


**Figure 18.**  
 Concentration profiles  $K$ , at  $x/H = 0.60, 1.20,$  and  $1.80$  and comparison with the Gaussian profile.

One practical application of this type of development is presented next. Wind tunnel tests were realized to evaluate some characteristics of the Alcântara Launch Center (ALC), which is the Brazilian gate to the space located at the north coast of Maranhão State, close to the Equator. Topographical local characteristics modify the parameters of incident atmospheric winds, and it can cause great influence on the gas dispersion process.

The topographical scale models were built to measure mean and fluctuating flow characteristics in order to understand the real behavior of ALC winds, and then, physical simulations of the effluent dispersion process were made using these scale models. The wind velocity was measured by a hot-wire anemometer, and the concentration fields in the proximities of a gas emission source were analyzed by an aspirating probe connected to the same anemometer system [23].

The dispersion process of the gases emitted from the launch center is illustrated in **Figure 19**. Different effluent conditions were tested to reproduce the emission caused by a rocket. Helium gas was used at the emission source to simulate the turbulent diffusion process. The results obtained were compared with previous full-scale measurements and computational evaluations considering the emission at ground level. A coherent behavior with the physics of the phenomena was observed [24].

#### 4.5 Wind tunnel tests of the flow in the wake of wind turbines

The interaction between the incident wind and wind turbines in a wind farm causes mean velocity deficit and increased levels of turbulence in the wake. The turbulent flow is characterized by the superposition of wind turbine wakes. A research work that included a series of wind tunnel tests to evaluate experimentally the spectral characteristics of turbulence in the wake of a wind turbine. Longitudinal



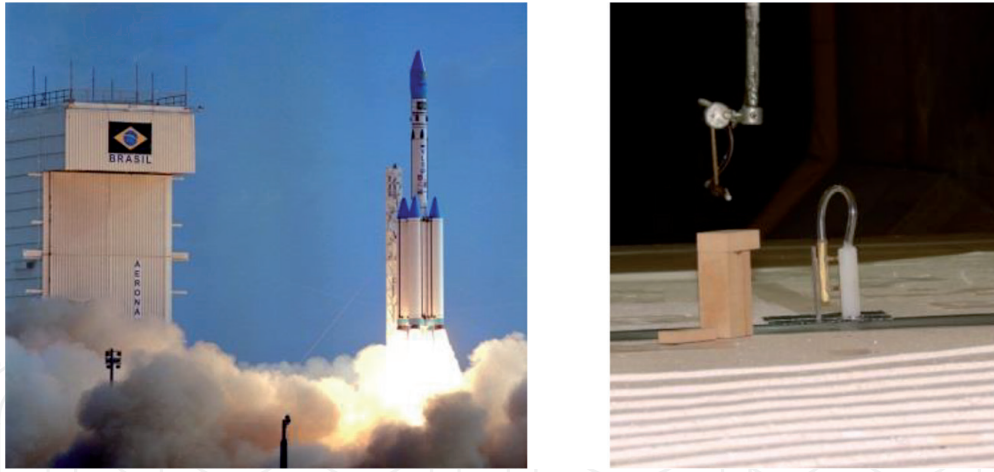


**Figure 19.** Launch of a space vehicle at the ACL, Maranhão, Brazil, and simulation of the dispersion process in the wind tunnel of the LAC/UFRGS.

velocity fluctuations were measured in the incident flow and in the wake of a wind turbine-reduced model in the test section of the UNNE wind tunnel. In these experiments, the adequacy of spectral technique and changes in the turbulence spectral composition of the incident wind and the wake were analyzed [25].

All longitudinal velocity fluctuation measurements were realized employing a neutral ABL flow obtained by the Counihan method similar to the full-depth simulation described in Section 2.2. The simulated incident wind corresponds to a power law profile with an exponent  $\alpha = 0.27$  and a gradient height  $z_g = 1.20$  m. Wind tunnel measurements were made using a hot-wire anemometer system. The wind turbine model corresponds to a three-bladed UNIPOWER wind turbine, with a tower height of 100 m and a rotor diameter of 100 m. The scale of the model is approximately 1/450, and the model height is 0.33 m. **Figure 20** shows the wind incident, making the turbine model rotate.

The rotational velocity of the wind turbine was estimated and remained nearly constant during the measurements, but the values of the dimensionless speed ratio  $\lambda$  ensure the similarity of phenomenon in the range of the proper operation of the generator. Vertical profiles of dimensionless mean longitudinal velocity  $U/U_{ref}$  measured in the incident wind and in the wake generated by the wind turbine are



**Figure 20.** Wind turbine model spinning during the wind tunnel test.

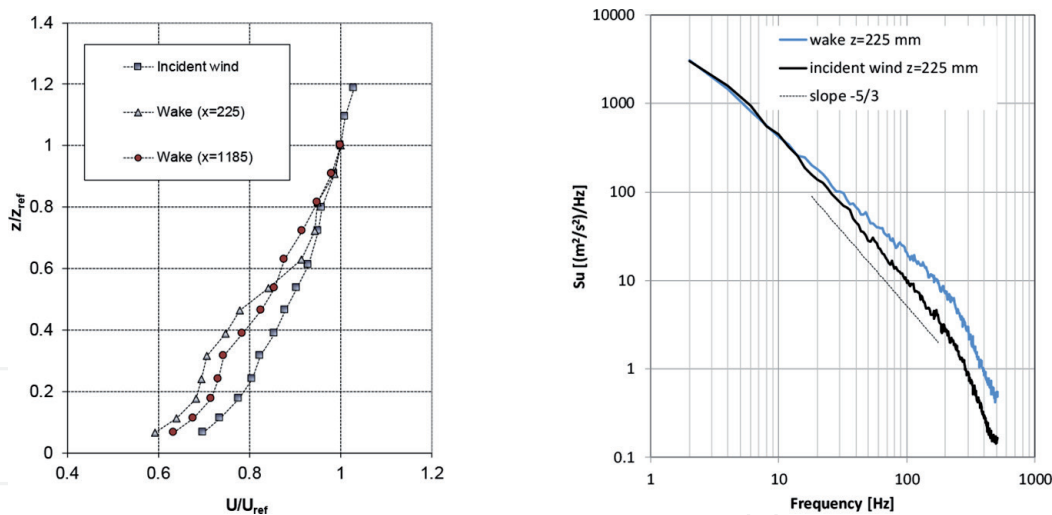


**Figure 21.** Vertical profiles of dimensionless mean longitudinal velocity and spectral comparison of the incident wind and the wake flow at  $z = 225$  mm.

indicated in **Figure 21**. Two profiles measured at locations  $x = 225$  and  $1185$  mm downwind of the plane determined by the rotor blades are included. The comparison of the characteristic spectra of the incident wind and those obtained in the wake are also shown in **Figure 21** and allow observing the changes in the energy fluctuation distribution. These changes are a product of the turbulence introduced by the wind generator. Measurements allowed to analyze the configuration of the spectra in different frequency ranges, the effect of analog signal filtering, and differences in the spectral behavior of the incident wind relative to wind in the wake of the turbine.

## 5. Concluding remarks

In this work, different boundary layer flows were experimentally analyzed. The BLF developed at the UNNE wind tunnel include a naturally developed boundary layer with the empty wind tunnel, a full-depth ABL generated by the Counihan method, and a part-depth ABL simulated by the Standen method.

A simplified analysis considering the depth of the neutral ABL of about 500 m compared with the gradient height (0.30 m) obtained for the empty tunnel implies a scale factor of 1/1650. In addition, turbulence intensity values inside the boundary layer are always minor than 10%, concluding that this boundary layer flow is not appropriate to wind engineering experiments.

Full-depth and part-depth simulations developed in the UNNE wind tunnel seem to show adequate performance. It is observed that values of measured turbulence intensity are lower than the values in the neutral atmosphere, mainly in the positions above, but other authors obtained similar results. Dimensionless spectral comparison indicates a deviation of the experimental results with respect to design spectra, but it is possible that parameters used to normalize the spectrum are not fully adequate. Some studies are being developed to verify this behavior.

Comparison of ABL flows obtained with low velocities and the ABL flow obtained with high velocity at the UFRGS wind tunnel indicates an acceptable behavior of the mean velocity and turbulence intensity distribution. Dimensionless spectra were not obtained for measurements with low velocities. However, a poor spectral definition was observed for measurements realized at the lowest velocity.

Five recent applications of ABL simulations in both wind tunnels (UNNE and UFRGS) are presented. A study of local wind loads on a high-rise building

considering the urban environment and the surrounding topography realized in the UNNE wind tunnel, where full-depth simulation flows were used. An experimental study of a low structure, specifically an airport where a part-depth boundary layer simulation developed at the UNNE wind tunnel, was utilized. Some wind tunnel applications to the aerodynamic analysis of cable-stayed bridges are shown where different incident flows were used.

Then, a pollutant atmospheric dispersion study realized in the UFRGS wind tunnel was shown. ABL flows obtained with low velocities were used to simulate the gas plume emission. A case study applied to the Brazilian Launch Center of Alcântara to evaluate the emitted gas dispersion process is also shown.

Finally, a recent wind tunnel study of the flow in the wake of wind turbines is presented. Measurements of the flow characteristics upwind and downwind of the turbine rotor were analyzed. Comparison of the turbulence spectra were also developed to evaluate the rotor effects on the turbine wake flow.

Also numerical methods are used mainly for forecasting and studying the dynamics of the airflow over large surfaces, usually with domains of several square kilometers. The Weather Research and Forecasting (WRF) model, which is a numerical weather prediction and atmospheric simulation system, is an example of this type of computational modeling. The size of the domain of the simulation of these models is much larger than the simulated spaces of boundary layer flows in a wind tunnel. However, some efforts are being made to link results from computational model and experimental data. In South America, for example, a WRF model was used by Puliafito et al. [26] to simulate mesoscale events of Zonda winds, and the obtained results were compared with meteorological data. The next objective of this research is to try the physical simulation of these events in a wind tunnel [27].

## **Acknowledgements**

This research was partially funded by Conselho Nacional de Desenvolvimento Científico e Tecnológico (CNPq, Brazil) and Secretaría General de Ciencia y Técnica, Universidad Nacional del Nordeste (SGCYT-UNNE, Argentina).

IntechOpen

IntechOpen

### Author details


Adrián R. Wittwer<sup>1\*</sup>, Acir M. Loredo-Souza<sup>2</sup>, Mario E. De Bortoli<sup>1</sup> and Jorge O. Marighetti<sup>1</sup>

<sup>1</sup> Facultad de Ingeniería, Universidad Nacional del Nordeste (UNNE), Resistencia, Argentina

<sup>2</sup> Laboratório de Aerodinâmica das Construções, Universidade Federal de Rio Grande do Sul (UFRGS), Porto Alegre, Brazil

\*Address all correspondence to: [a\\_wittwer@yahoo.es](mailto:a_wittwer@yahoo.es)

### IntechOpen

© 2019 The Author(s). Licensee IntechOpen. This chapter is distributed under the terms of the Creative Commons Attribution License (<http://creativecommons.org/licenses/by/3.0>), which permits unrestricted use, distribution, and reproduction in any medium, provided the original work is properly cited. 

## References

- [1] Arya S. Atmospheric boundary layers over homogeneous terrain. In: Plate EJ, editor. *Engineering Meteorology*. Amsterdam: Elsevier Scientific Publishing Company; 1982. pp. 233-266
- [2] Blessmann J. *O Vento na Engenharia Estrutural*. Porto Alegre, Brazil: Editora da Universidade. UFRGS; 1995
- [3] Cermak J, Takeda K. Physical modeling of urban air-pollutant transport. *Journal of Wind Engineering and Industrial Aerodynamics*. 1985;21:51-67
- [4] Surry D. Consequences of distortions in the flow including mismatching scales and intensities of turbulence. In: *Proceedings of the International Workshop on Wind Tunnel Modeling Criteria and Techniques in Civil Engineering Applications*; Gaithersburg, Maryland, USA. 1982. pp. 137-185
- [5] Cook N. Determination of the model scale factor in wind-tunnel simulations of the adiabatic atmospheric boundary layer. *Journal of Industrial Aerodynamics*. 1978;2:311-321
- [6] Vosáhlo L. *Computer Programs for Evaluation of Turbulence Characteristics from Hot-wire Measurements*. KfK 3743. Karlsruhe: Kernforschungszentrum Karlsruhe; 1984
- [7] Möller S. *Experimentelle Untersuchung der Vorgänge in engen Spalten zwischen den Unterkanälen von Stabbündeln bei turbulenter Strömung [dissertation]*. KfK 4501. Karlsruhe, RFA: Universität Karlsruhe (TH); 1988
- [8] Wittwer A, Möller S. Characteristics of the low speed wind tunnel of the UNNE. *Journal of Wind Engineering and Industrial Aerodynamics*. 2000;84:307-320
- [9] Counihan J. An improved method of simulating an atmospheric boundary layer in a wind tunnel. *Atmospheric Environment*. 1969;3:197-214
- [10] Standen N. A spire array for generating thick turbulent shear layers for natural wind simulation in wind tunnels. National Research Council of Canada. NAE. Report LTR-LA-94. 1972
- [11] Blessmann J. The boundary layer wind tunnel of UFRGS. *Journal of Wind Engineering and Industrial Aerodynamics*. 1982;10:231-248
- [12] Yassin M, Katob S, Ookab R, Takahashib T, Kounob R. Field and wind-tunnel study of pollutant dispersion in a built-up area under various meteorological conditions. *Journal of Wind Engineering and Industrial Aerodynamics*. 2005;93:361-382
- [13] Wittwer A, Loredou-Souza A, Oliveira M, De Bortoli M, Marighetti J. Análisis experimental de cargas de viento localizadas en un edificio de gran altura. In: *Memorias de XXXVI Jornadas Sudamericanas de Ingeniería Estructural*; Montevideo, Uruguay. 2014
- [14] Wittwer A, De Bortoli M, Natalini B, Marighetti J, Natalini M. Estudio de cargas de viento de la nueva terminal de pasajeros del Aeropuerto de Ezeiza mediante ensayos en túnel de viento. In: *Memorias de XXI Jornadas Argentinas de Ingeniería Estructural*; Buenos Aires, Argentina. 2010
- [15] Cook N. *The designer's guide to wind loading of building structures*. In: Part 1: Background, Damage Survey, Wind Data and Structural Classification. London, UK: Building Research Establishment; 1990
- [16] Loredou-Souza AM, Rocha MM. *Determinação Experimental*,

em Túnel de Vento, do Comportamento Aerodinâmico do Complexo Viário  
Jornalista Roberto Marinho/Octávio Frias de Oliveira, Fase III; Relatório LAC-UFRGS; Porto Alegre, Brazil; 2005

[17] Loredó-Souza AM, Rocha MM. Determinação experimental, em túnel de vento, do comportamento aerodinâmico do Complexo Viário Jornalista Roberto Marinho/Octávio Frias de Oliveira. Fase VI—Modelo aeroelástico completo; Relatório LAC-UFRGS; Porto Alegre, Brazil; 2007

[18] Wittwer A, Loredó-Souza A, Camaño Schettini E. Analysis of concentration fluctuations in a plume emission model. In: Proceedings of the 11th Americas Conference on Wind Engineering; June 22-26, Puerto Rico. 2009

[19] Wittwer A, Loredó-Souza A, Camaño Schettini E. Laboratory evaluation of the urban effects on the dispersion process using a small-scale model. In: Proceedings of the 13th International Conference on Wind Engineering. ICWE13; Amsterdam, The Netherlands. 2011

[20] Wittwer A, Loredó-Souza A, Camaño Schettini E, Castro H. Wind tunnel study of plume dispersion with varying source emission configurations. *Wind and Structures*. 2018;**27**(6):417-430

[21] Isyumov N, Tanaka H. Wind tunnel modelling of stack gas dispersion—difficulties and approximations. In: Proceedings of the fifth International Conference on Wind Engineering; Fort Collins, Colorado, USA; 1980

[22] Camaño Schettini E. Etude Expérimentale des Jets Coaxiaux avec Différences de Densité [Thèse de Docteur]. France: Institut National Polytechnique de Grenoble; 1996

[23] Wittwer A, Alvarez y Alvarez G, Demarco G, Martins L, Puhales F,

Acevedo O, et al. Employing wind tunnel data to evaluate a turbulent spectral model. *American Journal of Environmental Engineering*. 2016;**6**(4A):156-159

[24] Wittwer A, Loredó-Souza A, Oliveira M, Fisch G, De Souza B, Goulart E. Study of gas turbulent dispersion process in the Alcântara Launch Center. *Journal of Aerospace Technology and Management*. 2018;**10**:1-17

[25] Wittwer A, Dorado R, Alvarez y Alvarez G, Degrazia G, Loredó-Souza A, Bodmann B. Flow in the wake of wind turbines: Turbulence spectral analysis by wind tunnel tests. *American Journal of Environmental Engineering*. 2016;**6**(4A):109-115

[26] Puliafito E, Allende D, Mulena C, Cremades P, Lakkis S. Evaluation of the WRF model configuration for Zonda wind events in a complex terrain. *Atmospheric Research*. 2015;**166**:24-32

[27] Loredó-Souza A, Wittwer A, Castro H, Vallis M. Characteristics of Zonda wind in south American Andes. *Wind and Structures*. 2017;**24**(16):657-677